

Topside LPD17 Flow and Temperature Study with An Implicit Monolithic Scheme

F. Camelli, O. Soto, R.Löhner
School of Computational Sciences
Laboratory for Computational Fluid Dynamics
George Mason University, M.S. 4C7
Fairfax, VA 22030-4444, e-mail:fcamelli@gmu.edu

W. C. Sandberg, and R. Ramamurti
Laboratory for Computational Physics and Fluid Dynamics
Naval Research Laboratory
Washington, DC 20375-5344

Abstract

The present paper presents the results of a numerical study of the topside airwake flow and stack gas temperature field around the San Antonio class LPD 17. An LES simulation of the flow was performed using a Smagorinsky turbulence closure model. The time integration was implicit using a monolithic scheme. This study was performed for a 0 degree angle of attack of inflow. The computed results for the velocity agree well with the experimental data.

Introduction

The air flow over the complex geometry of a ship superstructure is incompressible, unsteady, and turbulent. Such a flow may be solved using large eddy simulation (LES) coupled with the appropriate turbulence model. A quantitative description of the flow unsteadiness in the landing area is crucial for aircraft operations, e.g. taking off and landing. The incorporation of the dynamics of the flow structures can add significantly to the realism of pilot training simulators. There have been a number of computational studies of ship topside airwake recently [3, 4, 5, 11, 13, 14, 15, 16]. We have carried out computational airwake studies which addressed helicopter landing [6], and stack gas flow and ingestion into ship spaces [7, 8]. The present study extends our previous airwake computation on the LPD-17 [13, 14] to include coupling the ship topside flow to the thermal transport and diffusion of the gas from multiple stacks. We examine not only the heat of the gas as an indicator of potential problems for topside equipment operation but also the particle trajectories and impingement zones which can be related to material degradation. The present study addresses the case for 0

degree angle of attack of the inflow, i.e. ship streaming into calm wind conditions.

Finite Element Formulation

The incompressible Navier-Stokes equations to be solved here are:

$$\frac{\partial \mathbf{u}}{\partial t} + (\mathbf{u} \cdot \nabla) \mathbf{u} - \nu \Delta \mathbf{u} + \nabla p = \mathbf{f} \quad \text{in } \Omega \times (0, t_f), \quad (1)$$

$$\nabla \cdot \mathbf{u} = 0 \quad \text{in } \Omega \times (0, t_f) \quad (2)$$

where Ω is the flow domain, t is the time variable, \mathbf{u} the velocity field, ∇ the gradient operator, ν the kinematic viscosity, Δ the Laplacian operator, p the pressure and \mathbf{f} the external body forces (i.e. the gravity and the Boussinesq forces).

Let $\boldsymbol{\sigma}$ be the viscous stress tensor and \mathbf{n} the unit outward normal to the boundary $\partial\Omega$. Denoting by an overbar prescribed values, the boundary conditions for (2) to be considered here are:

$$\begin{aligned}
\mathbf{u} &= \bar{\mathbf{u}} \text{ on } \Gamma_{\text{du}}, \quad p = \bar{p} \\
&\text{and} \\
\mathbf{n} \cdot \boldsymbol{\sigma} &= \bar{\mathbf{t}} \text{ on } \Gamma_{\text{nu}}, \\
\mathbf{u} \cdot \mathbf{n} &= \bar{u}_n, \quad \mathbf{n} \cdot \boldsymbol{\sigma} \cdot \mathbf{g}_1 = \bar{t}_1 \\
&\text{and} \\
\mathbf{n} \cdot \boldsymbol{\sigma} \cdot \mathbf{g}_2 &= \bar{t}_2 \text{ on } \Gamma_{\text{mu}}
\end{aligned} \tag{3}$$

for $t \in (t_0, t_f)$. The boundary $\partial\Omega$ has been considered split into three sets of disjoint components Γ_{du} , Γ_{nu} and Γ_{mu} , the latter being the part where mixed conditions are prescribed: the normal velocity and the tangent stresses. Vectors \mathbf{g}_1 and \mathbf{g}_2 (for the three-dimensional case) span the space tangent to Γ_{mu} . Finally, Γ_{du} and Γ_{nu} are the two disjoint components of $\partial\Omega$ where Dirichlet and Neumann boundary conditions for the velocity are prescribed. Compatible initial conditions have to be appended to problem (2)-(3).

The monolithic time-accurate formulation presented in [20, 18], was used to discretize the incompressible Navier-Stokes equations. Such a formulation can be written as follows: Given \mathbf{u}_h^n , find $(\mathbf{u}_h^{n+1}, p_h^{n+1}, \boldsymbol{\pi}_h^{n+1}, \boldsymbol{\xi}_h^{n+1})$ in $\mathbf{V}_h \times Q_h \times \tilde{\mathbf{V}}_h \times \tilde{\mathbf{V}}_h$ such that

$$\begin{aligned}
&\frac{1}{\delta t}(\mathbf{u}_h^{n+1,i} - \mathbf{u}_h^n, \mathbf{v}_h) + (\mathbf{u}_h^{n+\theta,i-1} \cdot \nabla \mathbf{u}_h^{n+\theta,i}, \mathbf{v}_h) \\
&\quad + (\nu \nabla \mathbf{u}_h^{n+\theta,i}, \nabla \mathbf{v}_h) + (\nabla p_h^{n+1,i-1}, \mathbf{v}_h) + \\
&(\tau(\mathbf{u}_h^{n+\theta,i-1} \cdot \nabla \mathbf{u}_h^{n+\theta,i} - \boldsymbol{\pi}_h^{n+\theta,i-1}), \mathbf{u}_h^{n+\theta,i-1} \cdot \nabla \mathbf{v}_h) \\
&\quad = (\mathbf{f}^{n+\theta}, \mathbf{v}_h) + (\boldsymbol{\sigma}^{n+\theta,i-1} \cdot \mathbf{n}, \mathbf{v}_h)_{\Gamma_{\text{mu}}}
\end{aligned} \tag{4}$$

$$\begin{aligned}
&\delta t(\nabla p_h^{n+1,i} - \nabla p_h^{n+1,i-1}, \nabla q_h) + \\
&\quad (\tau(\nabla p_h^{n+1,i} - \boldsymbol{\xi}_h^{n+1,i-1}), \nabla q_h) \\
&\quad = -(\nabla \cdot \mathbf{u}_h^{n+1,i}, q_h)
\end{aligned} \tag{5}$$

$$(\boldsymbol{\pi}_h^{n+\theta,i}, \tilde{\mathbf{v}}_h) = (\mathbf{u}_h^{n+\theta,i} \cdot \nabla \mathbf{u}_h^{n+\theta,i}, \tilde{\mathbf{v}}_h) \tag{6}$$

$$(\boldsymbol{\xi}_h^{n+1,i}, \tilde{\mathbf{v}}_h) = (\nabla p_h^{n+1,i}, \tilde{\mathbf{v}}_h) \tag{7}$$

$\forall(\mathbf{v}_h, q_h, \tilde{\mathbf{v}}_h, \tilde{\mathbf{v}}_h) \in \mathbf{V}_h \times Q_h \times \tilde{\mathbf{V}}_h \times \tilde{\mathbf{V}}_h$, where the intrinsic time step size is defined as:

$$\tau = \frac{h^2}{4\nu + 2\|\mathbf{u}\|h} \tag{8}$$

being h and $\|\mathbf{u}\|$ the elemental size and velocity norm, re-

spectively. The following notation has been used above:

$$\begin{aligned}
(\mathbf{a}, \mathbf{b}) &= \int_{\Omega} \mathbf{a} \cdot \mathbf{b} \, d\Omega \\
&\text{and} \\
(\mathbf{a}, \mathbf{b})_{\Gamma} &= \int_{\Gamma} \mathbf{a} \cdot \mathbf{b} \, d\Gamma
\end{aligned} \tag{9}$$

The superscript n and i stand for the time step counter and the block Gauss-Seidel iteration number into each time step, respectively, $0 < \theta \leq 1$ is the trapezoidal rule parameter ($\theta = 1$ backward-Euler and $\theta = 0.5$ Crank-Nicholson time discretization), the subscript h refers to the discrete functions, $\boldsymbol{\pi}$ and $\boldsymbol{\xi}$ are the projection into the finite element space of the pressure and convective terms, respectively, and the functional spaces \mathbf{V}_h and Q_h are the standard linear finite element ones.

In the above formulation, the advective effects are stabilized by the fifth LHS term of (4), which is the subtraction of the classical streamline diffusion term [2, 12] and its projection into the finite element space. The pressure is stabilized following the same idea (terms multiplies by τ in (5)): by adding to the weak incompressible equation the subtraction of the gradient of pressures and its projection.

If the one dimensional stencil of a nodal point k is developed for the advective terms (Galerkin plus stabilization), the following expression is found:

$$\mathcal{L}_k = \frac{1}{8}a(u_{k-2} - 8u_{k-1} + 6u_k + u_{k+2}) \tag{10}$$

where $a = u_h^{n+\theta,i-1}$ is the advective velocity, and $u_j = u_{h_j}^{n+\theta,i}$ the unknown. Using a Taylor expansion around u_k , it can be shown that this term represents the following formal second order discretization of the convective operator:

$$a \frac{du_k}{dx} = \frac{1}{h}\mathcal{L}_k - \frac{h^2}{6} \frac{d^3 u_k}{dx^3} + O(h^3) \tag{11}$$

In the same way, the one-dimensional stencil of the pressure stabilizing terms (see (5)) is:

$$\tau \left(\frac{p_{k+1} - p_k}{h} - \frac{p_{k+1} - p_{k-1}}{4h} - \frac{p_{k+2} - p_k}{4h} \right) \tag{12}$$

which can be re-written at the right hand side as:

$$-\frac{\tau}{h} \left(p_k - p_{k+1} + \frac{h}{2}(\nabla p_k + \nabla p_{k+1}) \right) \tag{13}$$

where ∇p_k is the second order finite difference gradient of p evaluated at nodal point k , this is $\nabla p_k = (p_{k+1} - p_{k-1})/2h$. The (13) term is exactly the same higher order term presented by Löhner et al. in [9, 10], and is equivalent to a fourth-order damping term for the divergence equation. If the contributions of the two edges surrounding the nodal point k are written down, it can be seen that the final LHS stencil for the equation k is:

$$S_k = \frac{\tau}{4h} (p_{k-2} - 4p_{k-1} + 6p_k - 4p_{k+1} + p_{k+2}), \quad (14)$$

which implies

$$S_k = \frac{\tau}{h} \frac{3}{12} h^4 \frac{d^4 p_k}{dx^4} + O(h^6). \quad (15)$$

Then, taking into account that τ is proportional to h or to h^2 for convective or viscous dominated flows respectively (see (8)), the pressure stabilizing term is formally at least a fourth order term.

REMARK 1: Note that the method is consistent. The solution of (1)-(2) is solution of (4)-(7), and when the mesh size h tends to zero, not only the stabilizing “viscosity” τ (see equation (8)) tends to zero, but also the stabilizing pressure and advective residual terms ($\nabla p_h^{n+1,i} - \xi^{n+1,i-1}$ and $\mathbf{u}_h^{n+\theta,i-1} \cdot \nabla \mathbf{u}_h^{n+\theta,i} - \pi_h^{n+\theta,i-1}$). In addition, if $\theta = 0.5$ is used for the trapezoidal rule (Crank Nicholson), it is formally second order accurate in time, and it is clear from the discrete form (4)-(7), that the steady-state solution does not depend on the time step size.

Turbulence Closures

Smagorinsky Model

The Reynolds-stress tensor given by $\tau_{ij} = -\overline{u_j^i u_i^j}$ is modeled by Equation (16) in the Smagorinsky closure [17].

$$\tau_{ij} = 2\nu_{tur} S_{ij} \quad (16)$$

$$S_{ij} = \frac{1}{2} \left(\frac{\partial U_i}{\partial x_j} + \frac{\partial U_j}{\partial x_i} \right) \quad (17)$$

where S_{ij} is the resolved strain rate and ν_{tur} is the Smagorinsky eddy viscosity given by

$$\nu_{tur} = (C_s h)^2 \sqrt{S_{ij} S_{ij}} \quad (18)$$

where h is the grid scale and C_s is the Smagorinsky coefficient that can be adjusted $0.10 < C_s < 0.24$.

Problem Description

The geometry of the LPD17 is illustrated in Figure (1). The dimensions of the ship are: 200 m in length, 30 m in width, and 50 m in height above the waterline.

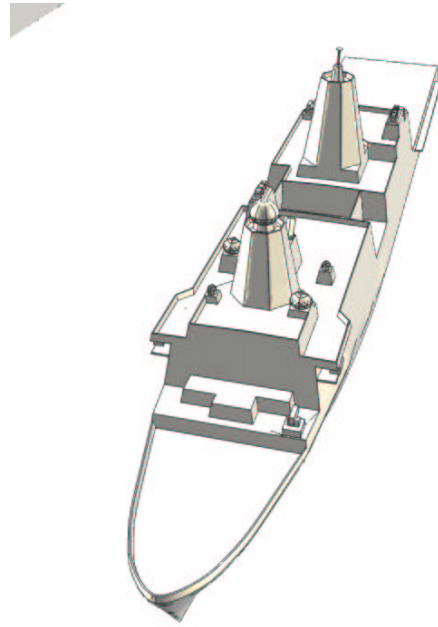


Figure 1: LPD17: geometry.

The ship has two main masts. The standard configuration of the ship has 5 diesel generator engine stacks (D/G), and 4 main propulsion engine stacks (M/P). These stacks are grouped as follow: 2 D/G behind the front mast, 2 M/P and 1 D/G in the right side of the ship between the two masts, and 2 M/P and 2 D/G in the left side before the landing deck. The flow rates and gas exit temperatures used in the simulation corresponded to the full power condition. The inflow condition is set to uniform flow with a velocity of 30 knots (15.43 m/s) assuming maximum ship speed. The inflow is in the x direction.

An initial critical and time consuming step that must be taken before airwake computations can begin is the generation of a 3-D surface model that accurately represents the ship and is suitable for CFD computations. The process of converting the design IGES files to the grid generation file format of the advancing front unstructured

grid generator for FEFLO was described in our earlier papers [13, 14]. Since the primary objective of the LPD-17 experimental airwake measurement project was CFD validation, great care was taken to ensure that our CFD geometry file was in agreement, to within construction accuracy, with the wind tunnel model. This highly accurate surface representation was the starting point for both the FEFLO computations [13, 14] and the FAST3D computations carried out by Guillot et al [3, 4].

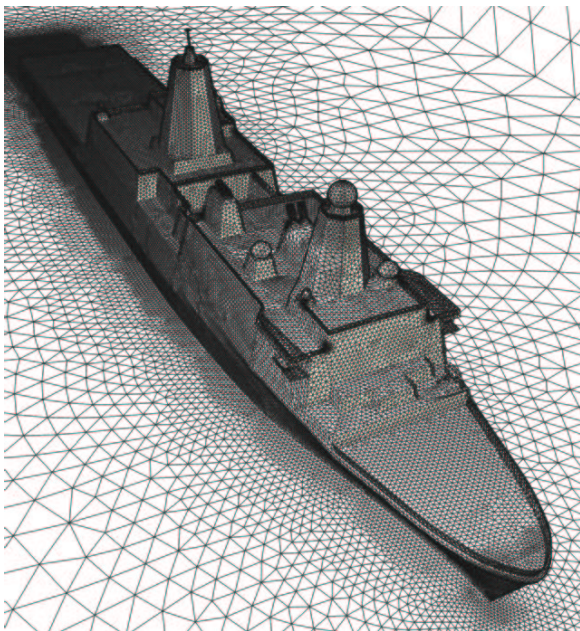


Figure 2: Front view of surface mesh.

We have, in the present study, carried out computations for about the same grid resolution used earlier and also at a much higher resolution. Two different grid resolutions were used, one coarser and other finer. The coarser mesh has 490,000 points and 2,720,000 tetrahedra. The finer mesh has 990,000 points and 5,640,000 tetrahedra. A view of the surface mesh for the coarser mesh is shown in Figure (2). A mid plane of the volume mesh is shown in Figure (3).

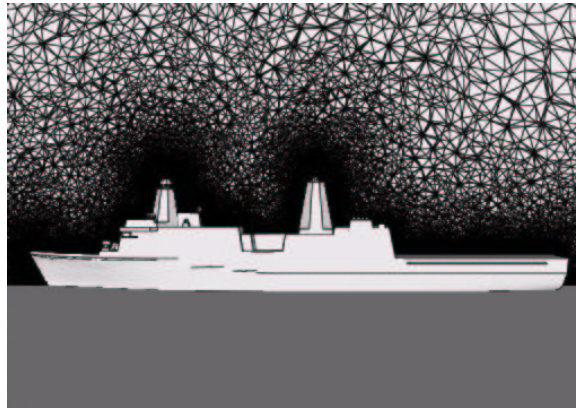


Figure 3: Mid plane of the volume mesh.

Results

LPD17 Topside Flow Study

The numerical simulation was performed with the implicit monolithic scheme presented in a previous Section. The time step was set to 0.01 s. The density was 1.225 kg/m^3 , and the viscosity was $1.789 \times 10^{-5} \text{ kg/m}\cdot\text{s}$. The Reynolds number based on the height of the ship is 5×10^7 . The flow is in the turbulent regime for this Reynolds number. Due to the unsteadiness and turbulent characteristics of the flow, an LES simulation was performed with the Smagorinsky turbulence model described in [17]. The Law of the Wall was used for the wall boundary condition.

In the first part of the run, a pseudo steady flow was established. After this state was reached, the flow was integrated for 90 s of real time. The whole run, including the initialization part, took approximately 2 weeks in 16 processors of an SGI 3800 shared memory machine at the Naval Research Laboratory, Washington DC. The pressure was set to the hydrostatic pressure. Buoyancy effects are considered in the simulation using the Boussinesq's approximation. A surface shading of the pressure field is shown in Figure (4). Snapshots of the velocity vectors and velocity contour lines in a cut plane are shown in Figure (5). The velocity vectors show large regions of recirculation and a very complicated flow pattern above the landing deck.

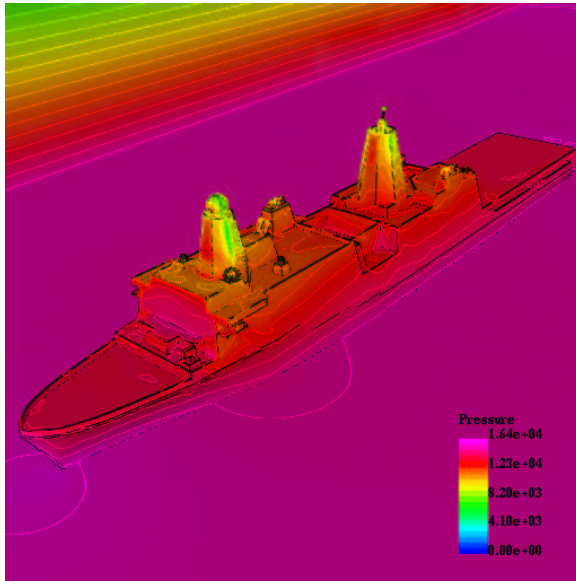


Figure 4: LPD17: hydrostatic pressure shading.

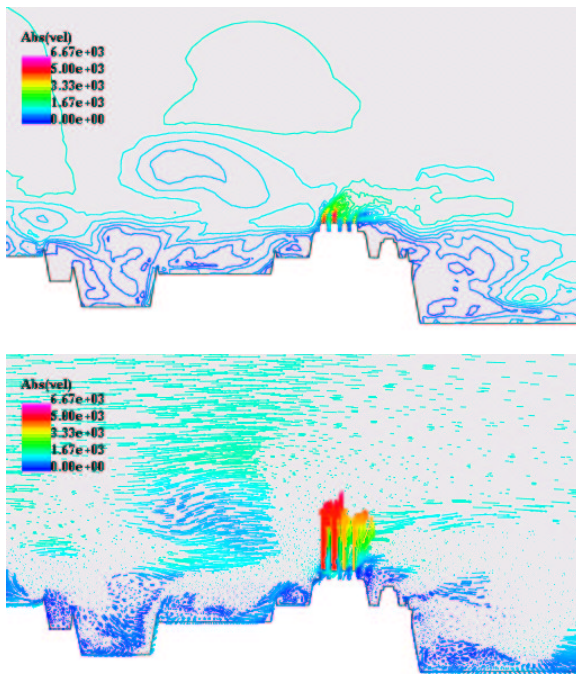


Figure 5: LPD17: velocity field in cut plane. Upper: velocity contour lines in cut plane. Lower: velocity vector plot in cut plane.

Two different techniques of visualization were applied to give a better understanding of the flow pattern. First, ribbons were used to visualize the flow. Figures (6) and (7) show two snapshots from different views. The ribbons are instantaneous streamlines of the flow [1]. This

technique helps to capture the areas with recirculation. Figure (6) shows a large recirculation above the landing deck. Figure (7) shows a particularly interesting feature. The ribbons indicate a pronounced crossflow from port to starboard near the middle of the ship. To visualize more clearly the time-varying trajectory of the gas and impingement zones on the superstructure, particles colored with temperature were released from the stacks. Figure (8) shows one such snapshot of released particles.

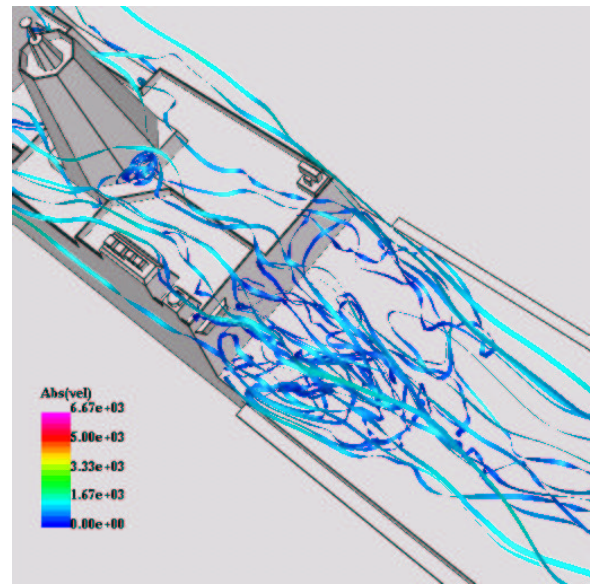


Figure 6: Ribbons colored with the velocity absolute value.

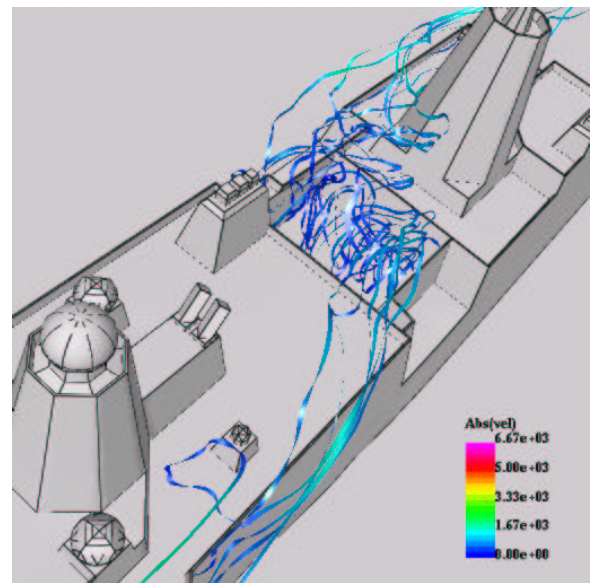


Figure 7: Ribbons colored with the velocity absolute value.

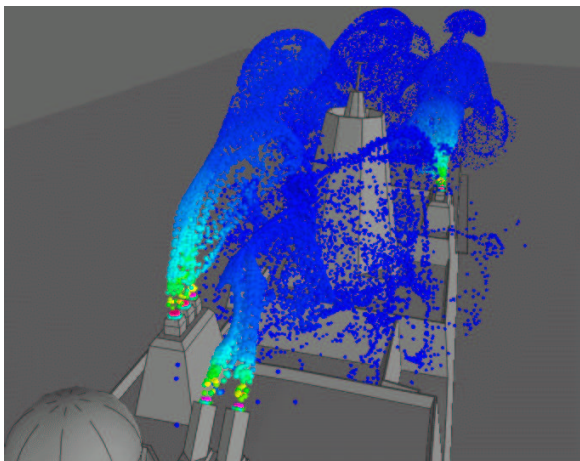


Figure 8: Particles colored with gas temperature.

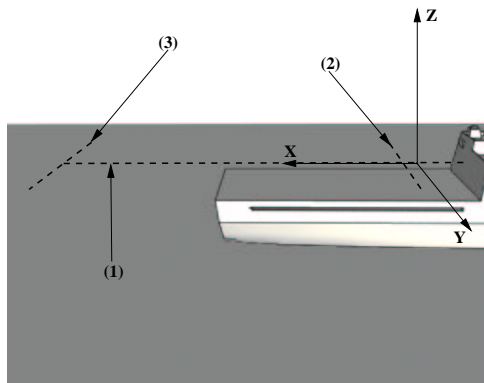


Figure 9: Position of station data time histories: side view of the flight deck. Experimental measurements were obtained at lines (1), (2), and (3)

Experimental velocity data from wind tunnel LDV measurements was available at the positions shown in Figure (9). The experimental velocities were averaged and compared with averaged numerical results. The numerical results were averaged over a period of 90 s. Figures (10) to (18) show the comparisons. The plotted velocities are in the x direction (u), in the y direction (v), and in the z direction (w). The crosses are the experimental data, the stars are the average of the numerical results, and the dash-dotted lines are the standard deviation of the numerical results. The numerical results agree fairly well with the experimental data for most of the plots. The numerical velocity in the x direction in the line station (2) (see Figure (13) shows a significant deviation from the experimental data at the center positions. One possible

explanation is the lack of resolution of the experimental instruments. This was also seen in our earlier computations [13, 14]. Experimental errors were not provided for the LDV data.

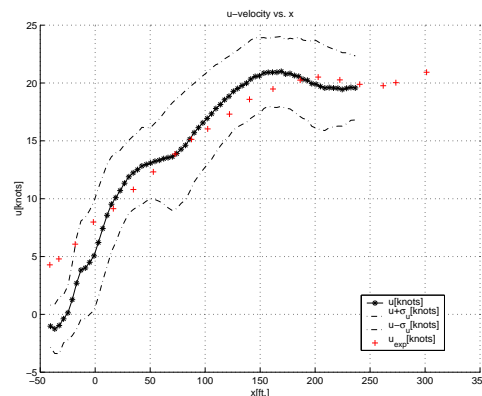


Figure 10: LPD17: u average velocity (1).

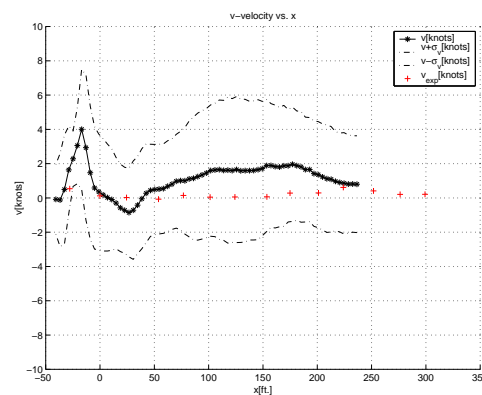


Figure 11: LPD17: v average velocity (1).

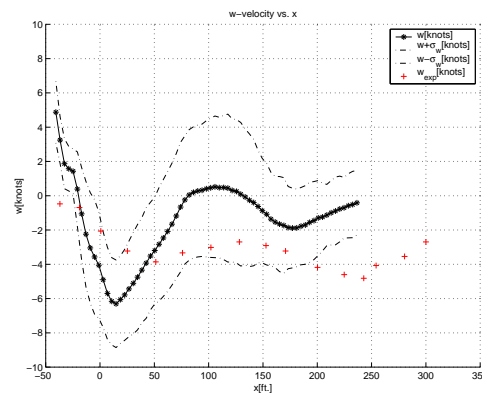


Figure 12: LPD17: w average velocity (1).

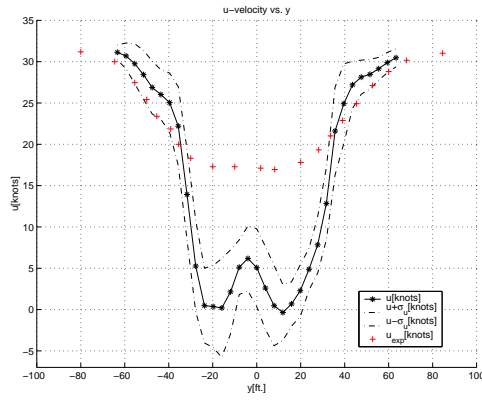


Figure 13: LPD17: u average velocity (2).

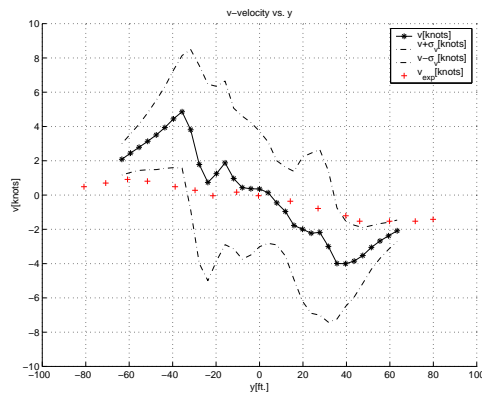


Figure 14: LPD17: v average velocity (2).

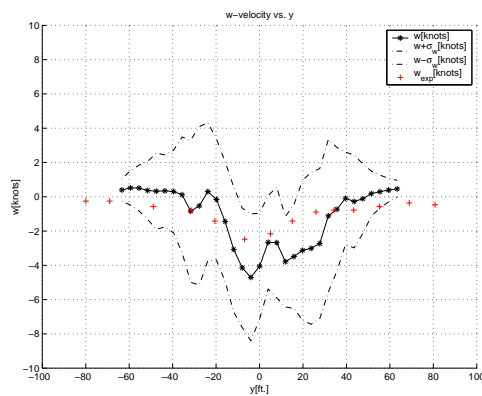


Figure 15: LPD17: w average velocity (2).

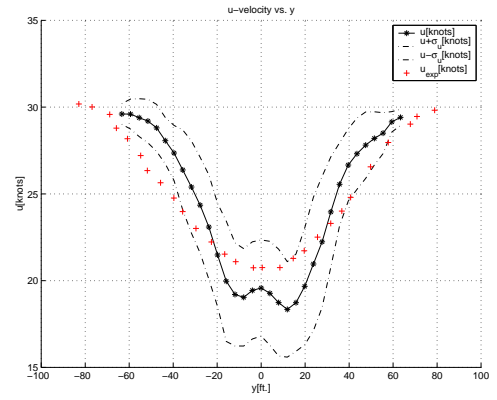


Figure 16: LPD17: u average velocity (3).

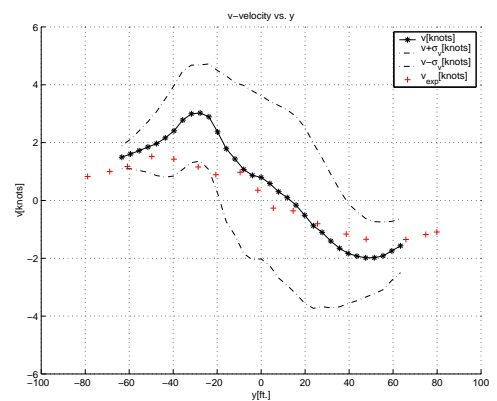


Figure 17: LPD17: v average velocity (3).

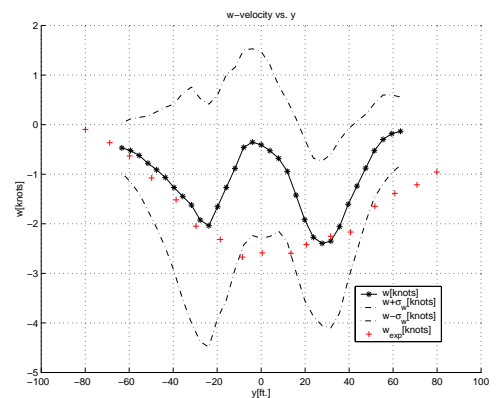


Figure 18: LPD17: w average velocity (3).

LPD17 Topside Temperature Study

The temperature study shows the importance of a proper grid resolution for a numerical simulation. The two meshes used are shown in Figures (19a) and (19b). Figure (19a) shows a cut plane of the coarse volume mesh.

The cut plane is in the centerplane where the group of 2 M/P stacks and 2 D/G stacks are. Figure (19b) shows the finer mesh in the same position. Figures (20a) and (20b) show the temperature iso-surface of level $50\text{ }^{\circ}\text{C}$. The coarse mesh shows more diffusion and less transport than the finer mesh. The numerical diffusion of a numerical scheme is proportional to the element (edge) size of the mesh. Figures (21a) and (21b) compare again the coarser and finer mesh results for the temperature at a same time step. Figure (21a) shows less transport of the temperature than the lower figure. Figure (21b) shows the buoyancy effects. A close view of the temperature surface is shown in Figure (22). The temperature on the aft mast is never greater than $50\text{ }^{\circ}\text{C}$ during the integration time. Temperature stations were placed near the mast and in the landing area. Table (1) shows the temperature values for the positions display in Figure (23).

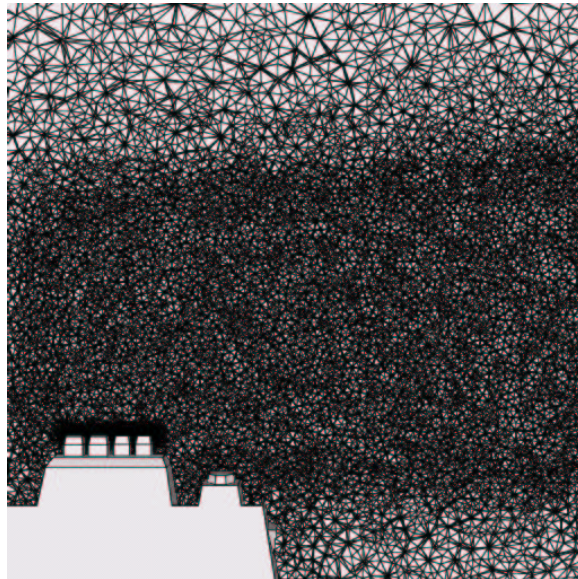


Figure 19b: Cut plane of volume finer mesh on the back stacks.

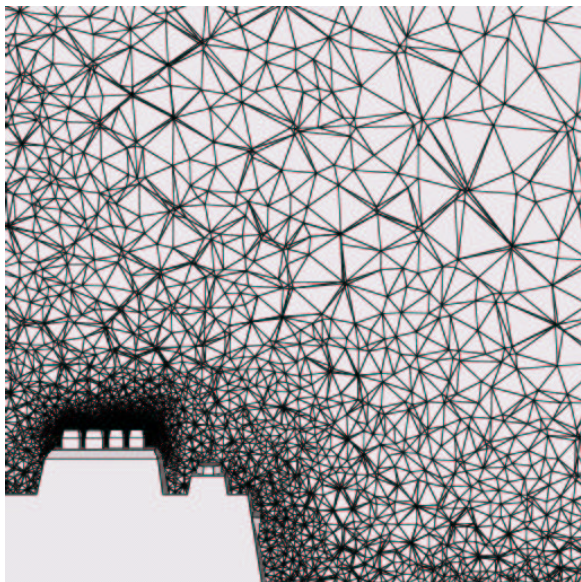


Figure 19a: Cut plane of volume coarser mesh on the back stacks.

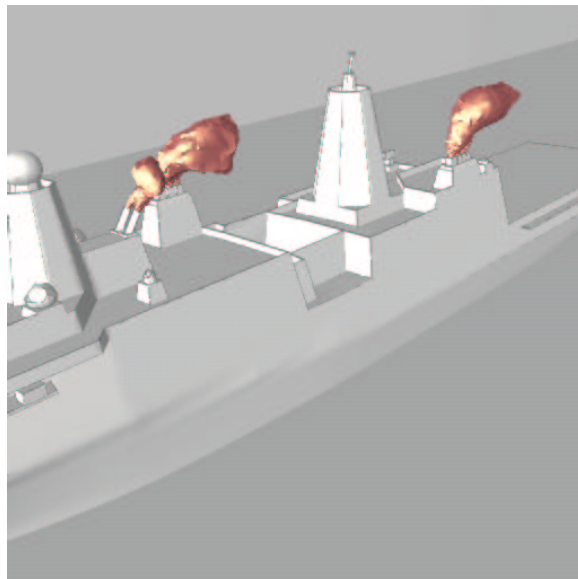


Figure 20a: Temperature iso-surface of level $50\text{ }^{\circ}\text{C}$. Run with the coarser grid.

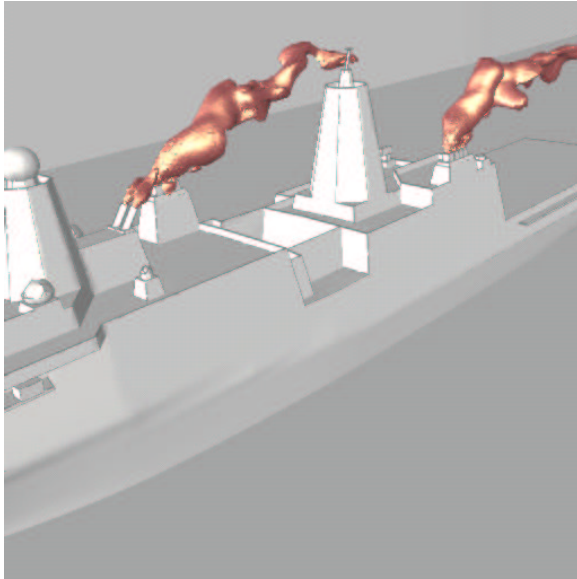


Figure 20b: Temperature iso-surface of level 50 °C. Run with the finer grid.

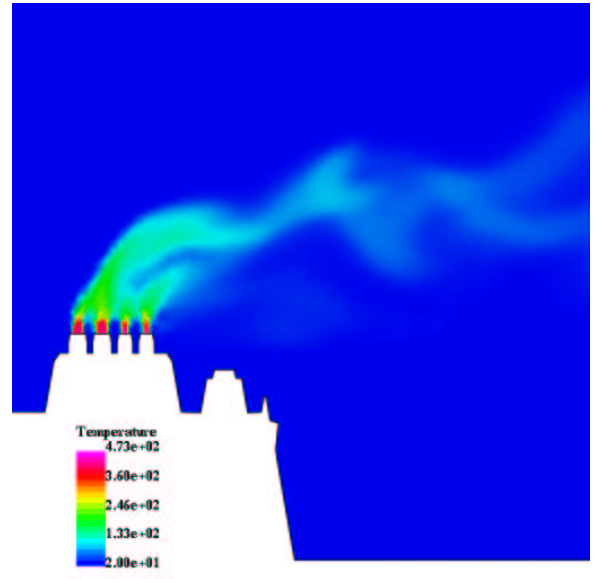


Figure 21b: Temperature distribution in a cut plane for the finer grid.

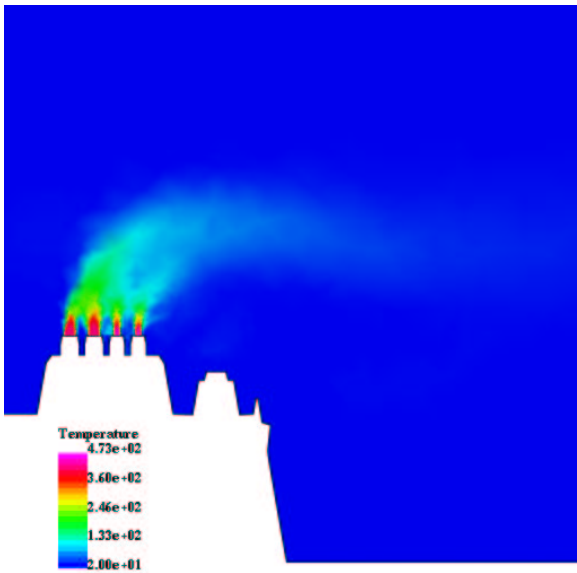


Figure 21a: Temperature distribution in a cut plane for the coarser grid.

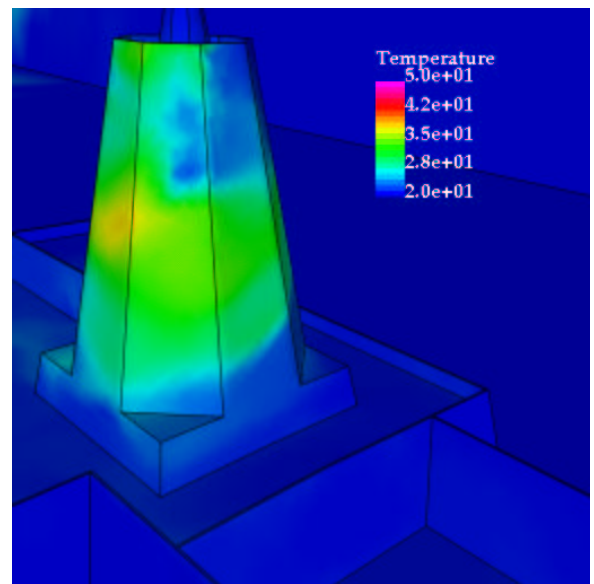


Figure 22: A close view of the surface temperature distribution.

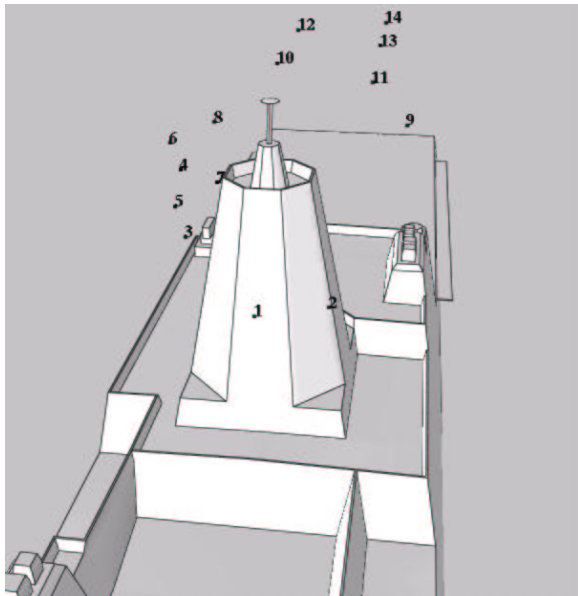


Figure 23: Position of temperature stations.

Station	Temperature [$^{\circ}\text{C}$]
1	30.55
2	32.12
3	79.44
4	38.98
5	33.48
6	63.88
7	43.25
8	39.00
9	87.00
10	37.71
11	40.68
12	34.16
13	55.11
14	47.23

Table 1: Temperature Stations.

Discussion and Outlook

The computed velocities were compared with wind tunnel data and showed good agreement. The complicated pattern of the flow was analyzed using several visualization techniques. These techniques provide a better understanding of the flow behavior. The computation time for this type of simulation is reasonable given the large amount of information obtained. The importance of grid resolution was demonstrated with the temperature study. The temperature study indicates that there is no temperature above 50°C in the region close to the aft mast of

the ship as it is shown in Figure (22). As continuation of the present work, we will study different angles of attack and different stack outlet conditions for the LPD17 and we are currently adding the study of concentration of gases emitted by the stacks for a different ship geometry (T-AKE 1).

References

- [1] G. K. Batchelor. *An introduction to fluid dynamics*. Cambridge: University Press, reprinted paperback edition, 1983.
- [2] A. Brooks and T. Hughes. Streamline upwind/Petrov-Galerkin formulations for convection dominated flows with particular emphasis on the incompressible Navier-Stokes equation. *Comp. Meth. Appl. Mech. Eng.*, 32:199–259, 1982.
- [3] M. J. Guillot and M. A. Walker. Unsteady analysis of the air wake over the LPD-17. *AIAA Paper 2000-4125*, 2000.
- [4] M. J. Guillot, M. A. Walker, K. Reader, R. Ramamurti, and W. C. Sandberg. LPD-17 topside aerodynamic study. Final Technical Report, NRL, 2000.
- [5] A. M. Landsberg, J. Boris, W. C. Sandberg, and T. R. Young. Naval ship superstructure design: Complex three-dimensional flows using an efficient parallel method. In *Proc. SCS Simulation Conference*, San Diego, CA, 1993.
- [6] A. M. Landsberg, J. Boris, W. C. Sandberg, and T. R. Young. Analysis of the nonlinear coupling of a helicopter downwash with an unsteady airwake. *AIAA Paper 1995-0047*, 1995.
- [7] A. M. Landsberg and W. C. Sandberg. DDG-51 Flt-IIA Airwake study part 3: Temperature field analysis for baseline and upgrade configuration. Memorandum Report 6401-00-8432, Naval Research Laboratory, Washington, DC, 2000.
- [8] A. M. Landsberg, W. C. Sandberg, T. R. Young, and J. Boris. DDG-51 Flt-IIA Airwake study part 2: Hangar interior flow. Memorandum Report 96-7898, Naval Research Laboratory, Washington, DC, 1996.
- [9] R. Löhner, C. Yang, E. Oñate, and S. Idelsohn. An unstructured grid-based, parallel free surface solver. *AIAA-97-1830*, 1997.

- [10] R. Löhner, C. Yang, E. Oñate, and S. Idelsohn. An unstructured grid-based, parallel free surface solver. *Applied Numerical Mathematics*, 31:271–293, 1999.
- [11] S. A. Polsky. A computational study of unsteady ship airwake. *AIAA Paper 2002-1022*, 2002.
- [12] R. Ramamurti and R. Löhner. A parallel implicit incompressible flow solver using unstructured meshes. *Computer and Fluids*, 5:119–132, 1996.
- [13] R. Ramamurti and W. C. Sandberg. LPD-17 top-side aerodynamic study: FEFLO. NRL Memorandum Report NRL/MR/6410–00-8498, Center for Reactive Flow and Dynamical Systems - Laboratory for Computational Physics and Fluid Dynamics - Naval Research Laboratory, October 2000.
- [14] R. Ramamurti and W. C. Sandberg. Unstructured grids for unsteady ship airwakes: A successful validation. *Naval Engineers Journal*, Feb 2002. Accepted.
- [15] K. R. Reddy, R. Toffoletto, and K. R. W. Jones. Numerical simulation of ship airwake. *Computers and Fluids*, 29:451–465, 2000.
- [16] A. Sharma and L. N. Long. Airwake simulations on an LPD-17 ship. *AIAA Paper 2001-2589*, 2001.
- [17] J. Smagorinsky. General circulation experiments. i. the basic experiment. *Monthly Weather Review*, 91:99–164, 1963.
- [18] O. Soto and R. Löhner. An implicit monolithic time accurate finite element scheme for incompressible flow problems. *AIAA-2001-2616*, 2001.
- [19] O. Soto, R. Löhner, and Cebal. A time-accurate implicit monolithic finite element scheme for incompressible flow problems. In *Proc. AIAA CFD Conference*, number 2616 in 2001, Anaheim, CA, June 2001.
- [20] O. Soto, R. Löhner, J. Cebal, and R. Codina. A time-accurate implicit-monolithic finite element scheme for incompressible flow problems. In *Proc. of ECCOMAS CFD 2001*, Swansea, Wales, September 4-7 2001.